

Plasma Sci. Technol. **20** (2018) 085603 (7pp) https://doi.org/10.1088/2058-6272/aac014

Development of a helicon-wave excited plasma facility with high magnetic field for plasma–wall interactions studies

Guilu ZHANG (张桂炉)[1,2], **Tianyuan HUANG** (黄天源)[1,2], **Chenggang JIN** (金成刚)[1,2,5,6], **Xuemei WU** (吴雪梅)[1,2,6], **Lanjian ZHUGE** (诸葛兰剑)[3] and **Hantao JI** (吉瀚涛)[4]

[1] College of Physics, Optoelectronics and Energy & Collaborative Innovation Center of Suzhou Nano Science and Technology, Soochow University, Suzhou 215006, People's Republic of China
[2] Key Laboratory of Modern Optical Technologies (Soochow University), Education of Ministry & Key Lab of Advanced Optical Manufacturing Technologies of Jiangsu Province & Jiangsu Key Laboratory of Thin Films, Soochow University, Suzhou 215006, People's Republic of China
[3] Analysis and Testing Center, Soochow University, Suzhou 215123, People's Republic of China
[4] Princeton Plasma Physics Laboratory, Princeton, New Jersey 08543, United States of America
[5] State Key Laboratory for Strength and Vibration of Mechanical Structures, Xi'an Jiaotong University, Xi'an 710049, People's Republic of China

E-mail: cgjin@suda.edu.cn and xmwu@suda.edu.cn

Received 4 December 2017, revised 17 April 2018
Accepted for publication 23 April 2018
Published 6 July 2018

Abstract

The high magnetic field helicon experiment system is a helicon wave plasma (HWP) source device in a high axial magnetic field ($\boldsymbol{B_0}$) developed for plasma–wall interactions studies for fusion reactors. This HWP was realized at low pressure ($5 \times 10^{-3} - 10$ Pa) and a RF (radio frequency, 13.56 MHz) power (maximum power of 2 kW) using an internal right helical antenna (5 cm in diameter by 18 cm long) with a maximum $\boldsymbol{B_0}$ of 6300 G. Ar HWP with electron density $\sim 10^{18}$–10^{20} m^{-3} and electron temperature ~4–7 eV was produced at high $\boldsymbol{B_0}$ of 5100 G, with an RF power of 1500 W. Maximum Ar^+ ion flux of 7.8×10^{23} $m^{-2}\,s^{-1}$ with a bright blue core plasma was obtained at a high $\boldsymbol{B_0}$ of 2700 G and an RF power of 1500 W without bias. Plasma energy and mass spectrometer studies indicate that Ar^+ ion-beams of 40.1 eV are formed, which are supersonic ($\sim 3.1 c_s$). The effect of Ar HWP discharge cleaning on the wall conditioning are investigated by using the mass spectrometry. And the consequent plasma parameters will result in favorable wall conditioning with a removal rate of 1.1×10^{24} N_2/m^2h.

Keywords: helicon wave plasma, high magnetic field, wall conditioning

(Some figures may appear in colour only in the online journal)

1. Introduction

Impurities and fuel particles are released due to strong plasma–wall interaction (PWI) in magnetically controlled fusion devices (such as stellarators and tokamaks), which affects the performance of the fusion plasma. With the view of controlling the surface state of the plasma-facing components (PFCs), and thus, the fluxes of fuel and impurities between the PFCs and the plasma, a wide variety of techniques are applied, which are called 'wall conditioning' [1, 2]. The present and future superconducting tokamaks such as ITER and DEMO, need efficient and alternative wall conditioning methods for the routine operation in the steady-state high axial magnetic field ($\boldsymbol{B_0}$), which prevents the use of conventional glow discharge conditioning (GDC) [3]. The wall conditioning using radio frequency (RF) plasma was carried out using ion cyclotron resonance (ICR) and electron cyclotron resonance (ECR) with the operating gas of He

[6] Authors to whom any correspondence should be addressed.

under the established $\boldsymbol{B_0}$. Recently, the ECR systems with the frequencies above 110 GHz on Textor-94, JT-60U and KSTAR were used for ECR plasma discharge cleaning under the $\boldsymbol{B_0}$ of 16500–37300 G [4, 5]. Typical electron temperature (T_e) and electron density (n_e) of ECR plasma were 1–10 eV and $3 \times 10^{18} - 2 \times 10^{19} m^{-3}$, respectively. The efficiency of H_2 outgas was found to be as large as 79% of that in He-GDC, which had been used in JT-60U. The ECR plasmas are almost toroidally homogeneous, while poloidally inhomogeneous, which is due to the exceedingly localized RF power deposition region which could make it hard to reach all the surface of the wall homogeneously. The ICR wall conditioning technique is rooted in low temperature and low density plasma discharge by RF pulses in noble or reactive gases [6]. This method has been tested in the tokamaks under $\boldsymbol{B_0} \sim$ 2000–40 000 G, RF power of up to hundreds of kW, and a working pressure of 1×10^{-3} to 0.1 Pa [7–9]. Plasma parameters were achieved in different ICR wall conditioning experiments ($n_e \sim 0.1–3 \times 10^{18}$ m^{-3}, ion temperature (T_i) $\sim$ 0.5–2 keV with high-energy tail (approximately several tens of keV), $T_e \sim$ 3–50 eV, and a low ionization degree ~1%–10%). The ICR wall conditioning experiments have been performed in TEXTOR [10], Tore Supra [11], W7-AS [12], HT-7 [13], JET [14], ASDEX-U [15], KSTAR [16], EAST [17] and LHD [18], and the significant progress has been obtained. The removing efficiency of ICR plasmas on impurity and hydrogen isotope particles is higher than ECR due to a more homogeneous distribution of poloidal plasmas. Nevertheless, ICR plasmas are poloidally asymmetric, such as the n_e at a factor 2–3 lower in the high-field side than in the low-field side [1, 2]. The very high frequency (VHF $\sim$ 140 MHz, higher than normally used in ICR) discharge was used for wall conditioning with hydrogen (H) atoms in the $\boldsymbol{B_0}$ of 750 G and the gas pressure of 2.7×10^{-2} Pa at the Uragan-2M torsatron. The characteristic value of n_e was $1–10 \times 10^{10}$ cm^{-3}, and the T_e varied in the range of 3–10 eV [19].

Compared with tokamaks, the plasma conditions of linear plasma generators can be carefully controlled and monitored for long periods of time. The properties of the plasma source can be tailored to study the phenomena of interest. They have long been used for the study of PWI under fusion-relevant conditions such as the MAGPIE at Australian National University [20], the DIONISOS experiment at Massachusettes Institute of Technology [21], PISCES facilities at UC San Diego [22], and the NAGDIS facilities at the University of Nagoya [23]. The achievable ion flux density in those devices is typically limited to 1×10^{23} m^{-2} s^{-1} in a steady-state low magnetic field. An advantage of the RF discharge, helicon wave plasma (HWP) discharge, could be produced in magnetic field. The helicon waves are bounded electromagnetic waves in the whistler wave range of frequencies, which is between the ion and electron cyclotron frequencies, with both left- and right-handed circular polarizations in magnetized plasma [24]. They are very important for high density plasmas, since they could propagate in higher density plasma up to 10^{20} m^{-3} [25, 26] than other waves in plasmas. High performance HWP discharges with light ions (such as deuterium (D), H, He and Ar), with $n_e > 10^{19}$ m^{-3} and gas utilization efficiency (η_g = ions out/atoms in ~100%) has been obtained. According to the dispersion relationship of the helicon wave, if the parallel wave number is fixed, the n_e is proportional to the $\boldsymbol{B_0}$ [25–27]. Therefore, higher $\boldsymbol{B_0}$ is expected to achieve higher n_e, which gives rise to high wall conditioning efficiency.

In this work, the experimental results of HWP steady-state discharge in a high $\boldsymbol{B_0}$ up to 5100 G are introduced. The influences of RF power and $\boldsymbol{B_0}$ on the HWP discharges are investigated. The experimental setup, including magnetic system, vacuum vessel, and HWP source are described. This HWP facility by appearing several measurements of n_e, T_e, and ion energy distribution in Ar plasmas is characterized.

2. HMHX system development

A novel PWI research facility, named high magnetic field helicon experiment system (HMHX), has been developed and constructed at Soochow University, as illustrated in [28]. The facility has been designed for the following experimental objectives: (a) HWP steady-state discharge with high $\boldsymbol{B_0}$ (>5000 G), (b) producing a high n_e ($>10^{19}$ m^{-3}) plasma in the PWI region to simulate the extreme environment of the edge regions in the fusion device, (c) working as a real-time test platform for developing high-efficiency wall conditioning technology.

2.1. Vacuum vessel

Figure 1 shows that the experimental setup consists of two main parts: an HWP source region and a PWI region [28]. The HWP source region is a stainless steel cylinder of 0.8-m-length and 0.2-m-diameter, which houses the whole antenna system. The HWP source region extension is the stainless steel PWI region of 0.4-m in both length and diameter, and it contains several fixed ports with a large silica window on the sides for various diagnostics. A movable stainless steel substrate (0.1-m-diameter) with a sample holder is installed inside the PWI region, which can be grounded, floated or biased by a DC and RF power source. The working gas is fed into the HWP source region and pumped out in the PWI region by a turbo-molecular pump (1200 L s^{-1} for N_2), which provides an ultimate pressure of 5×10^{-5} Pa; the pressure is measured in the PWI region by using an ionization gauge.

2.2. Antenna design and RF matching circuit

The RF power delivery system consists of three parts: an internal antenna, an RF power supply, and an impedance matching circuit. The internal antenna used in the experiment is an 18 cm-long, 3.5 cm-diameter, and right-handed Nagoya III helicon antenna that can launch $m = +1$ waves, which is parallel to the direction of the $\boldsymbol{B_0}$. It is made of a 6 mm-outer-diameter and 4 mm-inner-diameter copper tube and welded to the water-cooled RF feed-through, so that the antenna can be water cooled during high power operation. The antenna is

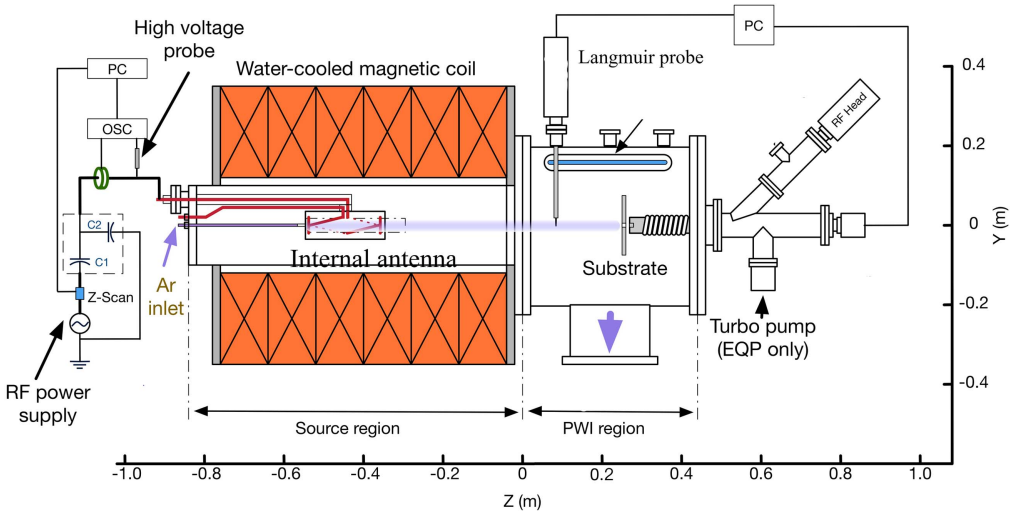

Figure 1. Diagram of the HMHX system showing its main parts: the magnets, the vacuum vessel, and the HWP source. The positions of the internal water-cooled antenna, Langmuir probe and EQP are indicated.

winded around a 22 cm-long, 3 cm-outer-diameter Al_2O_3 tube further covered with ceramic rings. Then all of the structures are sheathed in a stainless steel shield with active water-cooling. The working gas is fed into the HWP source tube through a Teflon tube connected to the left end of the shield (via a mass flow controller). The shield is electrically and mechanically connected to the grounded copper shield of the RF feed-through.

The RF power of 13.56 MHz (Rishige Company Ltd, PSG-IIIA) is supplied to the internal antennas through a typical L-type matching network, showing in figure 1. This matching network comprises two variable vacuum capacitors (C_1 = 15–500 pF, 10 kV and C_2 = 10–1000 pF, 10 kV). In order to measure the impedance of the circuit, the incident RF power (P_{in}), and the reflected RF power (P_{ref}), a Z-scan (Advanced Energy RF measurement system) is placed between the matching network and the RF power source. Since the P_{ref} is generally less than 1% of the P_{in} in experiments, the P_{in} is nearly equal to the absorbed RF power (P_{rf}). A 0.1 V A^{-1} Pearson current monitor (Model 110) is placed around the feed-through of internal antenna to measure the internal antenna current. For the measurement of the antenna voltage, a high voltage probe (P6015A, Tektronix) is connected to the antenna feed-through. The antenna effective resistance (R_{eff}) could be calculated from the P_{rf} and the averaged antenna current (I_{rms}, the root-mean square current), i.e., $R_{eff} = \frac{P_{rf}}{I_{rms}^2}$.

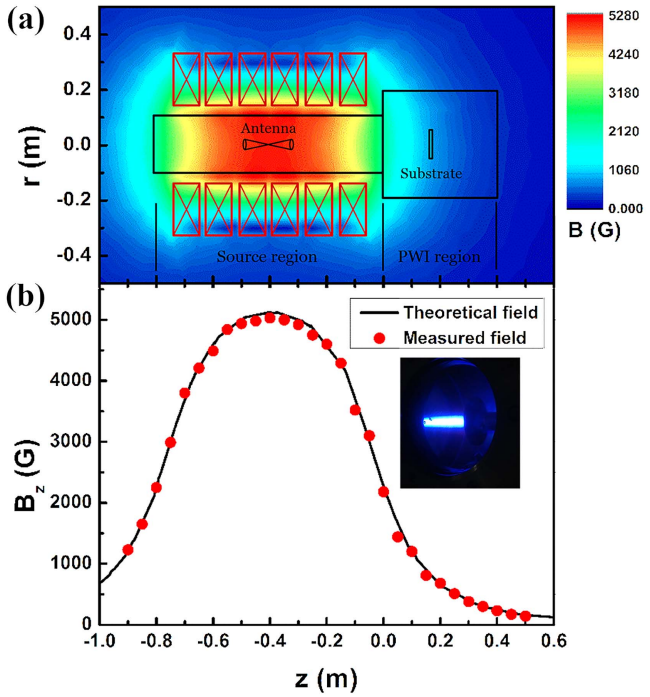

Figure 2. (a) COMSOL simulation of magnetic field strength configuration in the HMHX. (b) Magnetic field produced by the coil with 325 A, red dots are measured data, black line is simulation result from COMSOL, a photo of the HWP column in the PWI region is also shown.

2.3. Electromagnets

The magnet system of the device is designed for two essential purposes, plasma confinement and wave coupling, and it could also transport the plasma from the HWP source region into the PWI region. The magnet system consists of six sets of electromagnetic coils with water cooling, each with a 0.23-m-inter-diameter, 160 turns of copper tube covered with epoxy resin, and can produce ~6300 G flat top $\boldsymbol{B_0}$ by a passing 400 A current through them over a distance of 0.6 m. Iron yokes are also installed around the coils to confine and increase the $\boldsymbol{B_0}$ in the center of the source chamber. A set of two coils are connected to an independent DC power supply, so that the profile of the $\boldsymbol{B_0}$ could be easily modified by adjusting the current in different coils. Figure 2(a) shows that the $\boldsymbol{B_0}$ produced by the coils has been simulated numerically using COMSOL, and verified experimentally by taking measurements with a Tesla meter (TM-701, KANETEC),

showing in figure 2(b) for a coil current of 325 A. In this experiment, the $\boldsymbol{B_0}$ varying from 700 to 5100 G while the P_{rf} from 500 to 1500 W is used to study the influences of the $\boldsymbol{B_0}$ and the P_{rf} on the HWP discharge.

2.4. Diagnostics

A RF-compensated Langmuir probe (ESPION, Hiden Analytical Limited) is placed at 0.17 m downstream of the HWP source region interface (shown in figure 1), and is used to characterize the spatial plasma parameters in the PWI region, including plasma voltage (V_p), n_e and T_e. The parameters extracted from electron energy probability functions (EEPFs) provide key information including energy loss mechanisms, the electron heating, and the electron dynamics in plasmas, which are crucial to the diagnostic of HWP discharge, aiding in the understand of the physical behavior, which are calculated from the following formula [29]:

$$g(\varepsilon) = \frac{2m_e}{e^2 A}\left(\frac{2\varepsilon}{m_e}\right)^{\frac{1}{2}}\frac{d^2 I}{dV^2} \quad (1)$$

where m_e is the electron mass, e is the electron charge, $V = V_p - V_b$ (bias potential), I is electron current, A is the physical collecting area of the probe, ε is the electron energy. The plasma parameters of the n_e and the T_e are obtained as corresponding integrals of the EEPFs from the following formulae:

$$n_e = \int_0^\infty \varepsilon^{\frac{1}{2}} g(\varepsilon) d\varepsilon \quad (2)$$

$$T_e = \frac{2}{3n_e}\int_0^\infty \varepsilon^{\frac{3}{2}} g(\varepsilon) d\varepsilon. \quad (3)$$

A mass and energy analyzer (Hiden Analytical Limited, electrostatic quadrupole plasma (EQP)) is inserted into the plasma from the right flange of the PWI region chamber. A hole with 6 mm-diameter is drilled on the substrate, which allows the EQP probe to measure the ion energy distribution (IED) and characterize the distribution of the particle mass near the substrate. The mass spectrometer is operated in 'residual gas analyzer' (RGA) mode.

3. Results and discussion

3.1. Plasma production and characterization

Figure 3 shows an example of n_e by varying the P_{rf} with the $\boldsymbol{B_0}$ of 2700 G at the axis center in the PWI region chamber (i.e., $Y = 0$ and $Z = 0.17$ m in figure 1). From this figure, the n_e jumping to the order of 10^{18} m^{-3} with P_{rf} of 300 W is observed, which is well known as a mode transition behavior from inductively coupled plasma (ICP) [30] to HWP [31]. With further increasing P_{rf}, the n_e increases slightly and then achieves saturation. The T_e increases linearly with the P_{rf} increasing. The R_{eff} increases abruptly with the P_{rf} indicating marginally better coupling efficiency for an HWP versus a purely ICP source.

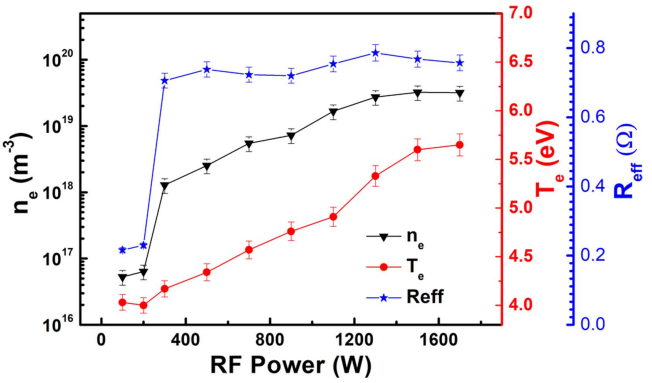

Figure 3. Variation of the n_e (black filled triangles), the T_e (red filled circles) and the R_{eff} (blue filled pentagons) with RF power for the $\boldsymbol{B_0}$ of 2700 G.

Figure 4(a) shows the variation of n_e and T_e with $\boldsymbol{B_0}$ under constant P_{rf} of 1500 W. The curve of n_e is approximately linear at low fields. However, the n_e decreases abruptly and then reaches saturation at high fields. In the condition of the $\boldsymbol{B_0} < 3100$ G, the n_e is approximately similar with that calculated from the dispersion relation of HWP [26]. However, with a further increase of $\boldsymbol{B_0} > 3500$ G, n_e gradually decreases and it is much lower than the calculated value. This discrepancy should be due to, for example, the lack of P_{rf} [27], which requires further investigation. The T_e decreases slightly in low fields, and has a similar way to the n_e in high fields. Figure 4(b) shows that V_p increases linearly with the $\boldsymbol{B_0}$ above 1000 G. For blue-core plasmas, the radial profiles n_e are shown in figure 4(c) (P_{rf} of 1500 W). It was noted that n_e reaches a maximum value at the axis, and decreases as it goes towards the edge. At the $\boldsymbol{B_0}$ of 700 G, the radial profile of n_e remains flat (black filled squares), which is a signature of ICP mode discharge. However, at higher $\boldsymbol{B_0}$ (above 700 G), peaked radial profile of density is observed, indicating the existence of HWP mode in the plasma. The full width at half maximum (FWHM) of the n_e peaks are observed to increase with the increasing $\boldsymbol{B_0}$, which is indicative of the increased radial confinement of plasma (figure 4(c)). As the higher $\boldsymbol{B_0}$ could confine the electrons for a longer time and help to transport the helicon wave into the whole plasma area, this means that higher ionization rate can be achieved.

Figure 5 shows that EEPFs exhibit a bi-Maxwellian distribution at the $\boldsymbol{B_0}$ of 700 G. As the $\boldsymbol{B_0}$ increases, the EEPFs evolve into a Maxwellian distribution due to the increase of both e-e collision and e-n collision. These trends in EEPF behavior are typical for high-density discharge plasma (independent of the specific electron heating mechanism in the discharge maintaining electric field, i.e. for DC, RF or microwave discharges). With increasing $\boldsymbol{B_0} \leqslant 2700$ G, the gentle slope of the tail temperature (T_e in the high energy range) indicates a production of 'tail' electrons in this region, in which high energy electrons transfer their energy to low energy electrons and the ionization process, inducing lower T_e and higher n_e. Boswell and Chen [25] have attributed the

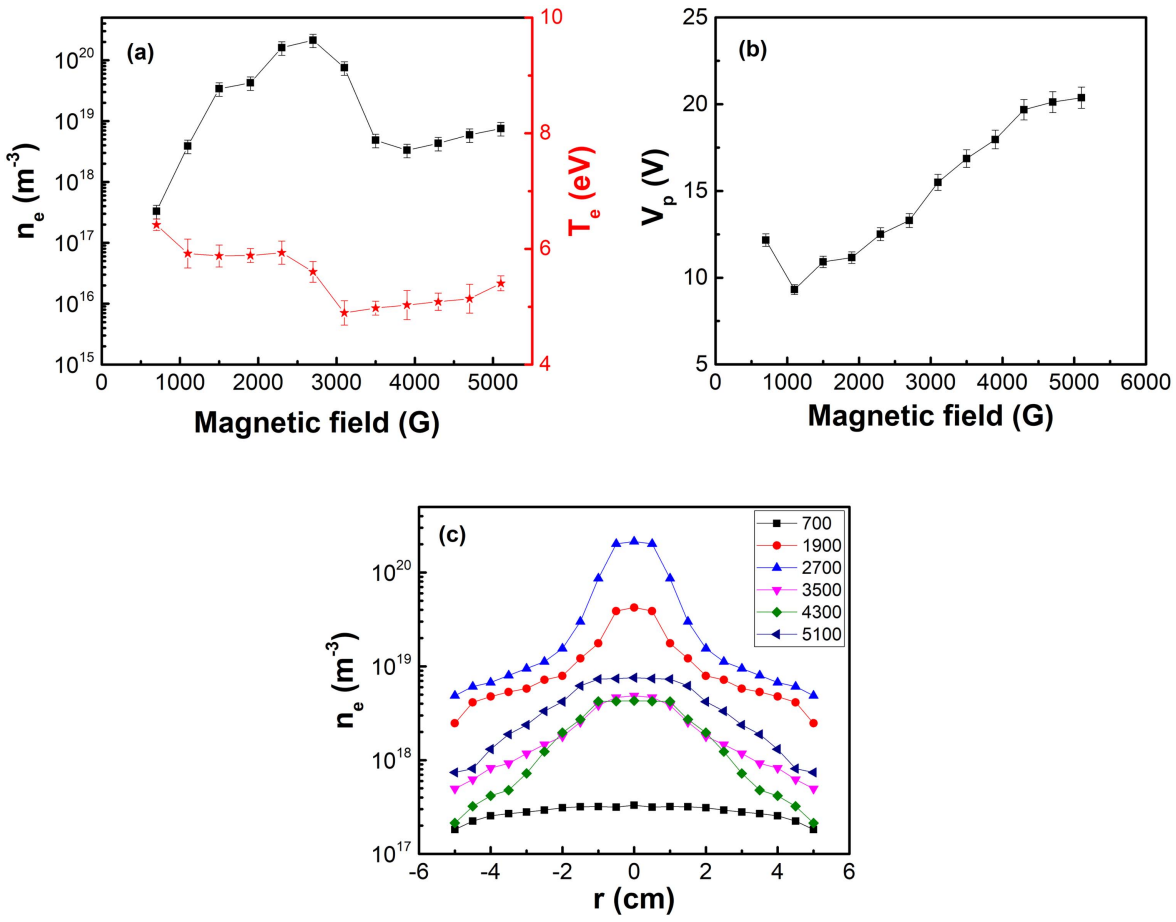

Figure 4. The measured plasma parameters: (a) the n_e (black filled squares) and the T_e (red filled pentagons), (b) the V_p, (c) Radial density profile as a function of $\boldsymbol{B_0}$.

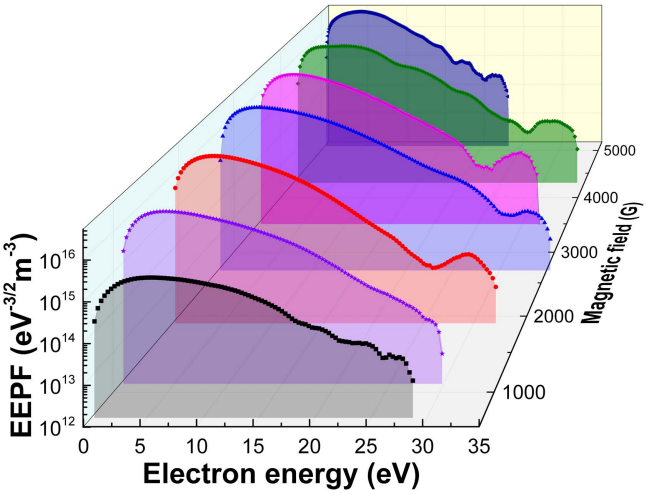

Figure 5. The measured EEPFs as a function of $\boldsymbol{B_0}$.

increase in the n_e with increasing the $\boldsymbol{B_0}$ to higher plasma confinement, which leads to improved coupling of the helicon wave to electrons and hence increasing the ionization efficiency. Therefore, it is noted that EEPFs could be adjusted by varying the $\boldsymbol{B_0}$. However, the EEPFs at $\boldsymbol{B_0} > 2700$ G, display a reduction of the high energy electrons and a decrease in density with respect to the $\boldsymbol{B_0}$ of 2700 G, which requires further studies.

The ion energy of Ar HWP has been further investigated by EQP. Figure 6 gives the ion energy distributions (IEDFs) of atomic Ar^+ as a function of the $\boldsymbol{B_0}$, showing the evolution of peak profiles and the drift of ion energy. While the IEDFs of atomic Ar^+ exhibit a two-peak structure. The lower energy peak is in response to the local plasma potential ($V_p \sim 13.3$ V), while the higher energy peak is indicative of ion-beam formation ($V_{beam} \sim 40.1$ V) at the $\boldsymbol{B_0}$ of 2700 G [32]. It is clear that a double layer (DL) is formed in Ar HWP discharges, which accelerates the atomic Ar^+ ions and creates an ion-beam at the downstream of the DL. Using the T_e of 5.6 eV for the current situation measured by the Langmuir probe, the ion-beam velocity and the Mach number could be calculated as [32]

$$v_{beam} = \sqrt{\frac{2e(V_{beam} - V_p)}{M_i}} = \sqrt{\frac{2eV_{DL}}{M_i}}. \quad (4)$$

The Mach number is about 3.1, i.e., supersonic. With increasing $\boldsymbol{B_0}$, the ion-beam energy raises from 28 eV to 56 eV. As the $\boldsymbol{B_0}$ is increased, there is an increase in the T_e and potential gradients, which results in larger ion-beam energies for all $\boldsymbol{B_0}$. It declares the ion-beam energy could be

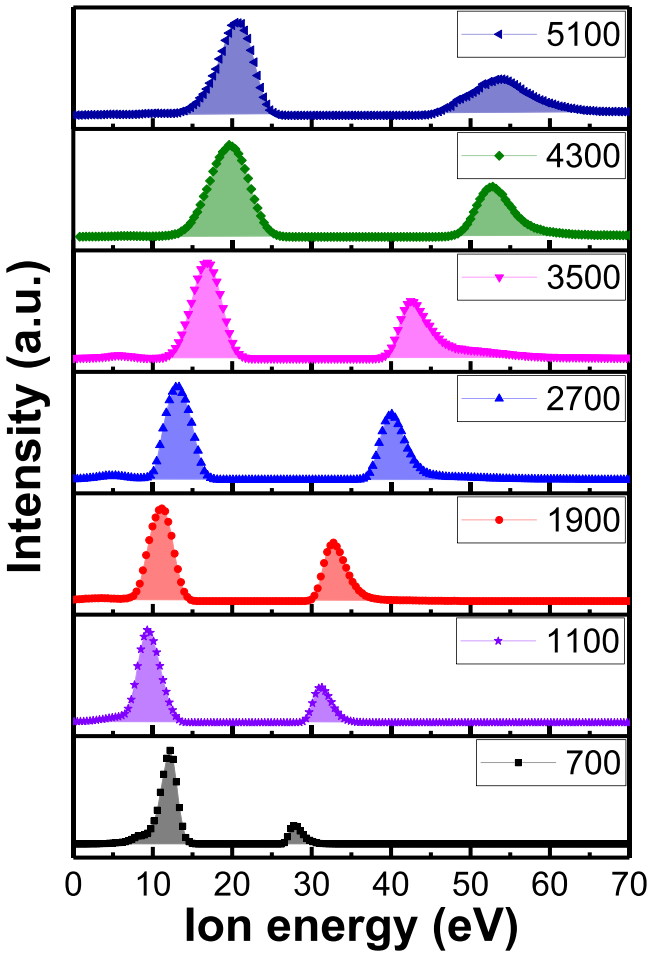

Figure 6. The normalized ion energy distributions of Ar^+ as a function of $\boldsymbol{B_0}$.

adjusted by varying the $\boldsymbol{B_0}$. The parameters are not expected to change much at the substrate, these results showed here are expected to give an evaluation of the ion energy parameter at the substrate.

3.2. HWP wall conditioning

The 0.1 m-diameter tungsten substrate as PFCs is exposed to high flux N_2 HWP ($\sim 10^{22}\,m^{-2}\,s^{-1}$) in 3 h. After N_2 retention in tungsten, Ar HWP discharge wall conditioning is carried out at the $\boldsymbol{B_0}$ of 2700 G and P_{rf} of 1500 W (plasma parameters: $n_e \sim 2 \times 10^{20}\,m^{-3}$, $T_e \sim 5.6$ eV, ion-beam energy ~40.1 eV). The bonding energy of impurity particle on the surface of the PFCs could be quite high, up to ~10 eV. Thus, the HWP with ion-beam energy ~ 40.1 eV discharge cleaning could effectively remove the impurities on the surface.

The direct and principal parameter of cleaning efficiency is the partial pressures evolution of neutral N_2 molecules during the wall conditioning, as illustrated in figure 7. From this figure, the partial pressure of the N_2 signal (AMU 28 and 14) increases slightly and then decreases abruptly at the time of 40 min when the plasma is off, indicating a significant wall conditioning effect. Moreover, the N_2 partial pressure after

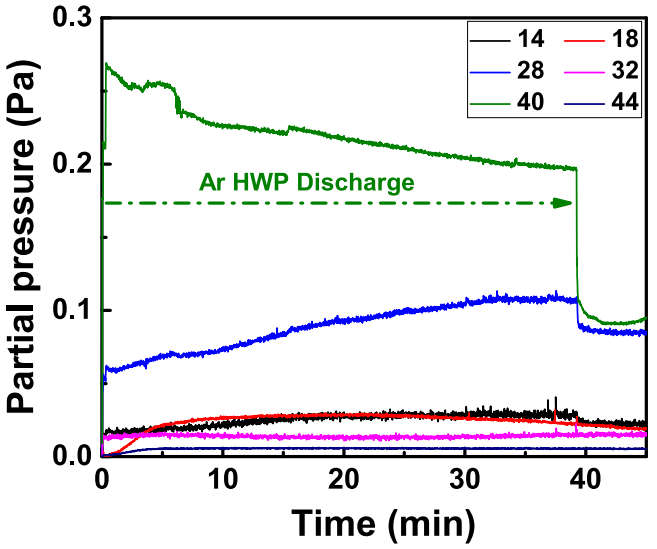

Figure 7. Partial pressure evolution during HWP wall conditioning.

HWP cleaning is higher than before, probably due to increased temperature of the tungsten substrate, and a longer time wall conditioning is required for the removal of nitrogen from tungsten substrate. The removal rate of HWP for N_2 is estimated by using the following formula:

$$RR_{N_2} = \frac{Q_{N_2}}{A_W \times t_p} = \frac{\int \Delta p_i \times s_i \mathrm{d}t}{A_W \times t_p} = 1.1 \times 10^{24}\,N_2/m^2h \tag{5}$$

where Δ_{Pi} is the increment of partial pressure of N_2 during HWP cleaning, S_i is the pumping speed for N_2, A_W is the surface area of tungsten target, and t_p is the duration of HWP discharge cleaning. The removal rate of HWP here is 3–4 orders higher than the normal removal rate of RF discharge for deuterium. It could be attributed to (1) high working pressure, (2) very localized HWP plasmas on tungsten substrate, and (3) high density plasmas for discharge cleaning, compared discharge cleaning plasmas in normal tokamaks. If HWP is applied to tokamaks in the future, plasma parameters would be much different from that shown in this paper, more effects are required for the usage of HWP on tokamak wall conditioning.

4. Conclusion

A novel HWP discharge device has been constructed to study PWI phenomena and work as a test bed for developing wall conditioning in fusion devices. The maximum n_e and flux of atomic Ar^+ are obtained at the $\boldsymbol{B_0}$ of 2700 G, which are $2.13 \times 10^{20}\,m^{-3}$ and $7.8 \times 10^{23}\,m^{-2}\,s^{-1}$, respectively. The Ar^+ ion-beams are formed, which are supersonic ($\sim 3.1 c_s$) and the ion-beam of 40.1 eV. As the $\boldsymbol{B_0}$ is increased, there is an increase in the potential gradients leading to larger ion-beam energies.

High removal rate of N_2, on average about $1.1 \times 10^{24}\,N_2/m^2h$, is obtained during the 40 min Ar HWP

discharge cleaning. Our present experimental results manifest a possible way for high flux of atomic Ar^+ and impacting ion kinetic energy in the range of 28–56 eV HWP discharge in high $\boldsymbol{B_0}$, and indicate its potential application in wall conditioning in steady-state superconducting fusion reactors such as ITER and DEMO.

Acknowledgments

This work was supported by the National Magnetic Confinement Fusion Science Program of China (Grant Nos. 2014GB106005 and 2010GB106000), National Natural Science Foundation of China (Nos. 11505123 11435009 11375126), and a Project funded by China Postdoctoral Science Foundation (No. 156455).

References

[1] Winter J 1996 *Plasma Phys. Controlled Fusion* **38** 1503
[2] de la Cal E and Gauthier E 2005 *Plasma Phys. Controlled Fusion* **47** 197
[3] Poschenrieder W, Staudenmaier G and Staib P 1980 *J. Nucl. Mater.* **93-94** 322
[4] Itami K *et al* 2009 *J. Nucl. Mater.* **390-391** 983
[5] Itami K *et al* 2013 *J. Nucl. Mater.* **438** S930
[6] Lyssoivan A *et al* 2011 *J. Nucl. Mater.* **415** S1029
[7] Douai D *et al* 2011 *J. Nucl. Mater.* **415** S1021
[8] Lyssoivan A *et al* 2005 *J. Nucl. Mater.* **337-339** 456
[9] Wauters T *et al* 2013 *Nucl. Fusion* **53** 123001
[10] Loewenhoff *et al* 2014 *Phys. Scr.* **T159** 010301
[11] Counsell G *et al* 2006 *Plasma Phys. Controlled Fusion* **48** B189
[12] Brakel R *et al* 2001 *J. Nucl. Mater.* **290-293** 1160
[13] Li J G *et al* 1999 *Nucl. Fusion* **39** 973
[14] Wauters T *et al* 2015 *J. Nucl. Mater.* **463** 1104
[15] Lyssoivan A *et al* 2007 *J. Nucl. Mater.* **363-365** 1358
[16] Lee D S *et al* 2017 *Fusion Sci. Technol.* **60** 94
[17] Gao X *et al* 2009 *J. Nucl. Mater.* **390-391** 864
[18] Takahashi H *et al* 2015 *J. Nucl. Mater.* **463** 1100
[19] Moiseenko V E *et al* 2014 *Nucl. Fusion* **54** 033009
[20] Blackwell B D *et al* 2012 *Plasma Source Sci. Technol.* **21** 055033
[21] Wright G M *et al* 2014 *Rev. Sci. Instrum* **85** 023503
[22] Jepu I *et al* 2015 *J. Nucl. Mater.* **463** 983
[23] Ohno N *et al* 2001 *Nucl. Fusion* **41** 1055
[24] Boswell R W 1984 *Plasma Phys. Controlled Fusion* **26** 1147
[25] Boswell R W and Chen F F 1997 *IEEE Trans. Plasma Sci.* **25** 1229
[26] Chen F F and Boswell R W 1997 *IEEE Trans. Plasma Sci.* **25** 1245
[27] Shinohara S and Mizokoshi H 2006 *Rev. Sci. Instrum.* **77** 036108
[28] Huang T Y *et al* 2016 *Sci. China Phys. Mech Astron.* **59** 645201
[29] Lieberman M A and Lichtenberg A J 2005 *Principles of Plasma Discharges and Materials Processing* 2nd edn (Hoboken, NJ: Wiley)
[30] Hopwood J 1992 *Plasma Sources Sci. Technol.* **1** 109
[31] Ellingboe A R and Boswell R W 1996 *Phys. Plasmas* **3** 2797
[32] Corr C S *et al* 2007 *Appl. Phys. Lett.* **91** 241501